

Proposal for a spin-polarized solar battery

Igor Žutić^{a)}

Department of Physics, University of Maryland at College Park, College Park, Maryland 20742

Jaroslav Fabian

Max-Planck Institute for the Physics of Complex Systems, Nöthnitzer Strasse 38, D-01187 Dresden, Germany

S. Das Sarma

Department of Physics, University of Maryland at College Park, College Park, Maryland 20742

(Received 27 April 2001; accepted for publication 3 July 2001)

A solar cell illuminated by circularly polarized light generates charge and spin currents. We show that the spin polarization of the current significantly exceeds the spin polarization of the carrier density for the majority carriers. Based on this principle, we propose a semiconductor spin-polarized solar battery and substantiate our proposal using analytical arguments and numerical modeling.

© 2001 American Institute of Physics. [DOI: 10.1063/1.1399002]

Illumination of a semiconductor sample by circularly polarized light results in a spin polarization of the carriers.¹ Optical spin polarization of both minority (optical orientation) and majority (optical pumping) carriers has been realized.¹ Introducing spin into semiconductors has also been reported by injecting spin-polarized carriers from a magnetic material (metal² or semiconductor³). Combined with the existence of reasonably long spin-relaxation times,^{4,5} this makes a strong case for all-semiconductor spintronics (traditional spintronic devices are metallic,⁶ suitable for their use in magnetic read heads and computer memory cells). The advantages of semiconductor spintronics⁷ would be an easier integration with the existing semiconductor electronics and more versatile devices; for example, information storage and processing could, in principle, be possible on the same spintronic chip. There already exist theoretical proposals for semiconductor unipolar spin transistors and spin diodes,^{8,9} and bipolar semiconductor devices based on the spin-polarized p - n junction.^{10,11} Related experimental advances, demonstrating spin-polarized light-emitting diodes³ and a gate-voltage tunable magnetization in magnetic semiconductors,¹² provide further motivation to explore all-semiconductor spintronics.

In this letter, we propose a spin-polarized solar battery as a source of both charge and spin currents. For its operation it is necessary to have spin imbalance in the carrier population (or in the corresponding components of current) as well as a built-in field which separates electron-hole pairs, created by illumination, producing voltage.¹³ We consider a particular implementation of a spin-polarized solar battery based on the concept of the spin-polarized p - n junction.¹¹ A circularly polarized light uniformly illuminates the sample (Fig. 1), generating spin-polarized carriers and spin-polarized charge current. An alternative geometry, using illumination only at the p region, has been considered in Ref. 11. We reveal by numerical modeling of drift-diffusion equations for spin and

charge transport that in the majority region current spin polarization is significantly enhanced over the carrier density polarization, and that spin polarization of the minority carriers near an ideal Ohmic contact is larger than in the bulk. By calculating the I - V characteristics for both charge and spin currents, we show that spin currents in the n region generally diminish with increasing forward voltage. We develop an analytical model based on spin diffusion to further support these findings.

Consider a GaAs sample at the room temperature, of length L (extending on the x axis from $x=0$ to $12\ \mu\text{m}$), doped with $N_A=3\times 10^{15}\ \text{cm}^{-3}$ acceptors on the left and with $N_D=5\times 10^{15}\ \text{cm}^{-3}$ donors on the right [the doping profile, $N_D(x)-N_A(x)$, is shown in Fig. 2]. The intrinsic carrier concentration is $n_i=1.8\times 10^6\ \text{cm}^{-3}$,¹³ and the electron (hole) mobility and diffusivity are 4000 (400) $\text{cm}^2\ \text{V}^{-1}\ \text{s}^{-1}$ and 103.6 (10.36) $\text{cm}^2\ \text{s}^{-1}$.¹³ The pair (band-to-band) recombination rate is taken to be $w=(1/3)\times 10^{-5}\ \text{cm}^3\ \text{s}^{-1}$, giving an electron lifetime in the p region of $\tau_n=1/wN_A=0.1\ \text{ns}$, and a hole lifetime in the n region of $\tau_p=1/wN_D=0.06\ \text{ns}$. The spin relaxation time (which is the spin lifetime in the n region) is $T_1=0.2\ \text{ns}$. In the p region electron spin decays on the time scale of $\tau_s=T_1\tau_n/(T_1+\tau_n)\approx 0.067\ \text{ns}$. The minor-

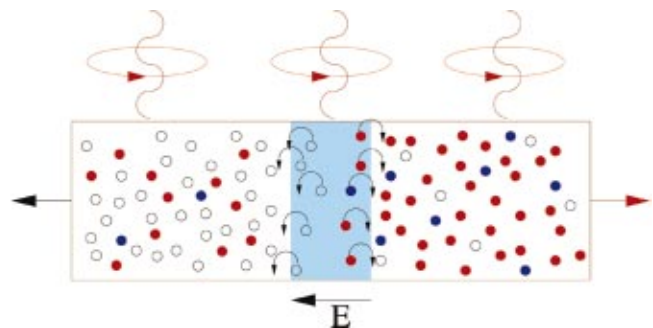


FIG. 1. (Color) Spin-polarized solar battery. Circularly polarized light creates electron-hole pairs. In the depletion region, by the built-in field E , spin-polarized electrons [red (blue)=spin up (down)] are swept to the n region (right), while the unpolarized holes (empty circles) are swept to the p region (left). A uniform illumination is assumed throughout the sample, giving rise to spin-polarized current (both spin and charge flow).

^{a)}Electronic mail: igor@cooperon.umd.edu

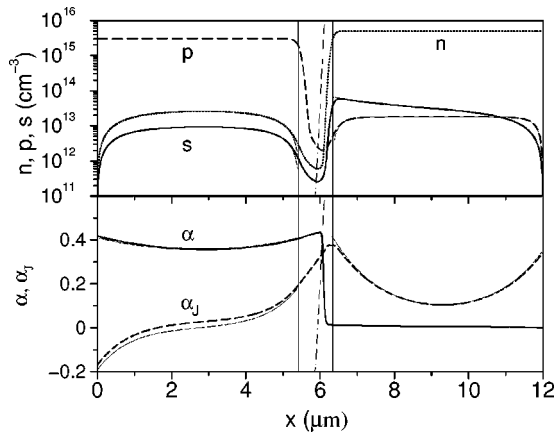


FIG. 2. Calculated spatial profiles of (top) carrier densities n and p , spin density s , and (bottom) electron and current spin polarizations α and α_J . The thin dashed lines show the doping profile $N_D(x) - N_A(x)$ (not to scale), and the two vertical lines at $x_p \approx 5.4$ and $x_n \approx 6.3$ indicate the depletion layer boundaries. The thin lines accompanying the numerical curves are analytical results for an ideal spin-polarized solar cell (if not visible, they overlap with the numerical results).

ity diffusion lengths are $L_n = (D_n \tau_n)^{0.5} \approx 1 \mu\text{m}$ for electrons in the p region, and $L_p = (D_p \tau_p)^{0.5} \approx 0.25 \mu\text{m}$ for holes in the n region. The spin decays on the length scale of $L_s^p = (D_n \tau_s)^{0.5} \approx 0.8 \mu\text{m}$ in the p and $L_s^n = (D_n T_1)^{0.5} \approx 1.4 \mu\text{m}$ in the n region. At no applied voltage, the depletion layer formed around $x_d = L/2 = 6 \mu\text{m}$ has a width of $d \approx 0.9 \mu\text{m}$, of it $d_p = (5/8)d$ in the p side and $d_n = (3/8)d$ in the n side.

Let the sample be uniformly illuminated with a circularly polarized light with photon energy higher than the band gap (bipolar photogeneration). The pair generation rate is chosen to be $G = 3 \times 10^{23} \text{cm}^{-3} \text{s}^{-1}$ (which corresponds to a concentrated solar light of intensity about $1 \text{W cm}^{-2} \text{s}^{-1}$), so that in the bulk of the p side there are $\Delta n = G \tau_n \approx 3 \times 10^{13} \text{cm}^{-3}$ nonequilibrium electrons and holes; in the n side the density is $\Delta p = G \tau_p = 1.8 \times 10^{13} \text{cm}^{-3}$. The band structure of GaAs allows a 50% spin polarization of electrons excited by a circularly polarized light, so that the spin polarization at the moment of creation is $\alpha_0 = G_s/G = 0.5$, where $G_s = G_\uparrow - G_\downarrow$ is the difference in the generation rates of spin-up and -down electrons. For a homogeneous doping, the spin density in the p side would be $s_p = G_s \tau_s \approx 1 \times 10^{13} \text{cm}^{-3}$, while in the n side $s_n = G_s T_1 \approx 3 \times 10^{13} \text{cm}^{-3}$. Holes in GaAs can be considered unpolarized, since they lose their spin on the time scale of momentum relaxation (typically, a picosecond). The physical situation and the geometry are illustrated in Fig. 1.

We solve numerically the drift-diffusion equations for inhomogeneously doped spin-polarized semiconductors¹¹ to obtain electron and hole densities n and p , spin density $s = n_\uparrow - n_\downarrow$ (where n_\uparrow and n_\downarrow are spin-up and -down electron densities), and charge J and spin $J_s = J_\uparrow - J_\downarrow$ (where J_\uparrow and J_\downarrow are spin-up and -down electron charge currents) current densities. We consider ideal Ohmic contacts attached at both ends of the sample, providing infinite carrier and spin recombination velocities (so that both nonequilibrium carrier densities and spin density vanish at $x=0$ and $x=L$). Our sample is large enough (compared to L_n , L_p , and L_s) to distinguish the bulk from the boundary effects, so the behavior of more realistic boundary conditions (which would include finite

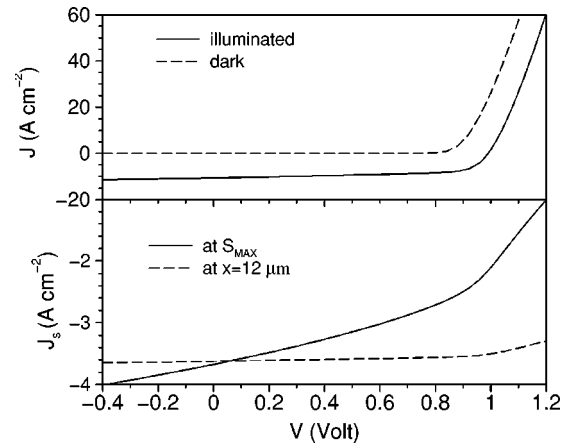


FIG. 3. Calculated I - V curves for charge currents (top: a solar cell in the dark and under illumination) and spin currents (bottom: the solid curve is for the spin current at the point in the n region where s is maximum, see Fig. 2, and the dashed curve is for J_s at the right end, $x = 12 \mu\text{m}$).

surface recombination velocities for both nonequilibrium carriers and spin) can be readily deduced from our results.

Calculated spatial profiles of carrier and spin densities, as well as carrier and current polarizations $\alpha = n/s$ and $\alpha_J = J_s/J$, are in Fig. 2. There is no applied voltage V , but the illumination produces a reverse photocurrent $J_{\text{photo}} = -eG(L_n + L_p + d) \approx -11 \text{A cm}^{-2}$ (see, also, Fig. 3). The behavior of the carrier densities is the same as in the unpolarized case (spin polarization in nondegenerate semiconductors does not affect charge currents, as diffusivities for spin-up and -down carriers are equal). The spin density essentially follows the nonequilibrium electronic density in the p side, sharply decreases in the depletion layer, while then rapidly increasing to a value larger than the normal excitation value in the n side, s_n . We interpret this as a result of spin pumping through the minority channel:¹¹ electron spin excited within the distance L_p^s from the depletion region, as well as generated inside that region, is swept into the n side by the built-in field, thus pumping spin polarization into the n region. In the rest of the n region, the spin density decreases, until it reaches zero at the right boundary. Carrier spin polarization α is reasonably high in the p side, but diminishes in the n side. [Note that in the geometry considered in Ref. 11 (top of Fig. 1), for a higher illumination intensity and short junction, the spin polarization remains almost unchanged through the depletion layer, a result of a much more effective electronic spin pumping.] The current polarization, however, remains quite large throughout the sample. It changes sign in the p region [note that $\alpha_J = J_s/J$, and since $J(V=0) = J_{\text{photo}} < 0$ is a constant, α_J shows the negative profile of the spin current], and has a symmetric shape in the n region, being much larger than α .

The profile of the carrier densities can be understood from the ideal solar cell model, based on minority carrier diffusion, and Shockley boundary conditions^{13,14} (which, for $V=0$, state that the nonequilibrium carrier density vanishes at the edges of the depletion layer). We do not write the formulas here, but we plot the analytical results in Fig. 2. The behavior of $s(x)$ can be understood along similar lines. Outside the depletion region we can neglect the electric field as far as spin transport is considered (one does not distin-

guish minority and majority spins—spin is everywhere out of equilibrium, and it can be treated similarly to minority carrier densities). The equation for spin diffusion is $D_n d^2 s/dx^2 = (wp + 1/T_1)s - G_s$. Consider first the p region. The boundary conditions are $s(0) = 0$ (the ideal Ohmic contact) and $s(x_p) = 0$, where $x_p = x_d - d_p$ is the point where, roughly, the depletion layer begins (see Fig. 2). The latter condition is an analogue of the Shockley condition that says that the photogenerated minority carrier density vanishes at the edges of the depletion layer, as carriers generated there are immediately swept into the other side of the layer by the built-in field. The same reasoning holds for spin, as spin is carried by the photogenerated electrons. The resulting spin density is

$$s(x) = s_p \left[\frac{\cosh(\xi_p) - 1}{\sinh(\xi_p)} \sinh(\xi) - \cosh(\xi) + 1 \right], \quad (1)$$

where $\xi = x/L_s^p$ and $\xi_p = x_p/L_s^p$. The spin current $J_s = \alpha J = eD_n ds/dx$. These analytical results, plotted in Fig. 2, agree with numerical calculation. Note that near the Ohmic contact spin polarization $\alpha(x \rightarrow 0) = \alpha_0(\tau_s/\tau_n)^{0.5} \approx 0.41$, which is larger than the bulk value of $\alpha_0(\tau_s/\tau_n) \approx 0.33$. The change in sign of J_s is related to the increase of s with increasing x , at small x , and then decrease close to the depletion layer. The current polarization is $\alpha_j(0) = -\alpha_0 L_s^p / (L_n + L_p + d) \approx -0.19$ and $\alpha_j(x_p) = -\alpha_j(0)$.

In the n region, the right boundary value is that of an Ohmic contact, $s(L) = 0$, but at the left it is a finite value $s(x_n) = s_0$ (where x_n is the depletion region boundary with the n side, $x_n = x_d + d_n$), determined below. The solution of the diffusion equation is

$$s(x) = s_n \left[\frac{\cosh(\eta_n) - 1 + s_0/s_n}{\sinh(\eta_n)} \sinh(\eta) - \cosh(\eta) + 1 \right], \quad (2)$$

where $\eta = (L - x)/L_s^n$ and $\eta_n = (L - x_n)/L_s^n$. To obtain s_0 , consider the physics which leads to its final value. In an ideal case, all the electron spin generated in the p region within the distance L_s^p from the depletion layer, as well as generated within the depletion layer, flow without relaxation into the n region. Then, the boundary condition for the spin current at x_n reads $J_s(x_n) = -eG_s(L_s^p + d)$. Since, at the same time, $J_s(x_n) = eD_n ds/dx|_{x_n}$, from Eq. (2) we obtain $s_0 = s_n [1 + \tanh(\eta_n)(L_s^p + d)/L_s^n - 1/\cosh(\eta_n)]$. In general, for a long junction ($\eta_n \gg 1$), $s_0 = G_s T_1 [1 + (L_s^p + d)/L_s^n]$, and the enhancement of spin due to the minority electron spin pumping is particularly large for reverse biased samples with large d . For a short junction ($\eta_n \ll 1$), $s_0 = s_n \eta_n (L_s^p + d)/L_s^n$, and the spin at x_n is solely due to electron spin pumping (but its value is smaller than for a long junction). In our case $s_0 \approx 2.2s_n$, and $s(x)$ [Eq. (2)], plotted in Fig. 2, gives very good agreement with the numerical data. Spin polarization of the current at the Ohmic contact is $\alpha_j(L) = \alpha_0 L_s^n / (L_n + L_p + d) \approx 0.33$, while that at x_n is $\alpha_j(x_n) = \alpha_0 [(L_s^p + d)/(L_n$

$+ L_p + d)] \approx 0.39$. Current polarization is much larger than carrier polarization, since both spin and charge currents are mainly diffusive. If only the p region would be illuminated¹¹ with photogenerated spin density G_s , the induced spin density in the n region would be $s_0 = G_s (T_1 \tau_s)^{0.5} \tanh(\eta_n)$. This is purely the minority-electron spin pumping effect. It is most effective for long junctions, where the spin amplification is $s_0/s_p = (T_1/\tau_s)^{0.5} = (1 + T_1/\tau_n)^{0.5}$. At low temperatures T_1 can be larger than τ_n by orders of magnitude, and so spin amplification can be significant.

Finally, in Fig. 3 we plot the I - V characteristics of the charge and spin currents. The resulting charge I - V curve under illumination can be, as in standard solar cells, understood as the effect of superposition¹³ of the negative short circuit current (reverse photocurrent J_{photo}) and the dark current, exponentially increasing with forward voltage. The total charge current vanishes at the open-circuit voltage of about 1 V. As the spin current is *not* conserved (it varies in space), we choose two points to represent it on the I - V plot. One is the value of J_s at the right boundary, the other at the point where spin is maximum (at the right edge of the depletion layer; this is an important point when a short junction would be considered). Both values decrease in magnitude with increasing voltage, as a result of decreasing of the effect of spin pumping from the nonequilibrium minority electrons. This is much more pronounced in the case of J_s at maximum s , which is most sensitive to the electronic pumping, as it varies with d (which decreases with increasing voltage).

This work was supported by DARPA and the U.S. O.N.R.

¹ *Optical Orientation*, edited by F. Meier and B. P. Zakharchenya (North-Holland, New York, 1984).

² P. R. Hammar, B. R. Bennett, M. J. Yang, and M. Johnson, Phys. Rev. Lett. **83**, 203 (1999).

³ R. Fiederling, M. Kleim, G. Reuscher, W. Ossau, G. Schmidt, A. Waag, and L. W. Molenkamp, Nature (London) **402**, 787 (1999); Y. Ohno, D. K. Young, B. Beschoten, F. Matsukura, H. Ohno, and D. D. Awschalom, *ibid.* **402**, 790 (1999); B. T. Jonker, Y. D. Park, B. R. Bennett, H. D. Cheong, G. Kioseoglou, and A. Petrou, Phys. Rev. B **62**, 8180 (2000).

⁴ J. M. Kikkawa and D. D. Awschalom, Phys. Rev. Lett. **80**, 4313 (1998).

⁵ J. Fabian and S. Das Sarma, J. Vac. Sci. Technol. B **17**, 1708 (1999).

⁶ G. A. Prinz, Science **282**, 1660 (1998).

⁷ S. Das Sarma, J. Fabian, X. D. Hu, and I. Žutić, Superlattices Microstruct. **27**, 289 (2000); IEEE Trans. Magn. **26**, 2821 (2000); LANL Preprint cond-mat/0105247, Solid State Commun. (to be published).

⁸ S. Datta and B. Das, Appl. Phys. Lett. **56**, 665 (1990).

⁹ M. E. Flatte and G. Vignale, Appl. Phys. Lett. **78**, 1273 (2001).

¹⁰ S. Das Sarma, J. Fabian, X. D. Hu, and I. Žutić, 58th Device Research Conference (IEEE, Piscataway, NJ, 2000), p. 95, and LANL Preprint cond-mat/0006369.

¹¹ I. Žutić, J. Fabian, and S. Das Sarma, LANL Preprint cond-mat/0103473, Phys. Rev. B (to be published).

¹² H. Ohno, D. Chiba, F. Matsukura, T. Omiya, E. Abe, T. Dietl, Y. Ohno, and K. Ohtani, Nature (London) **408**, 944 (2000).

¹³ A. L. Fahrenbruch and R. H. Bube, *Fundamentals of Solar Cells* (Academic, New York, 1983).

¹⁴ I. Žutić, J. Fabian, and S. Das Sarma, LANL Preprint cond-mat/0106085.